Lorena R. Lizarraga-Valderrama[1]

Rinat Nigmatullin[1]

Caroline Taylor[2]

John W. Haycock[2]

Frederik Claeyssens[2]

Jonathan C. Knowles[3,4]

Ipsita Roy[1]

[1] Applied Biotechnology Research Group, Department of Life Sciences, Faculty of Science and Technology, University of Westminster, London, UK

[2] Department of Materials Science and Engineering, Kroto Research Institute, Sheffield, UK

[3] Division of Biomaterials and Tissue Engineering, UCL Eastman Dental Institute, London, UK

[4] Department of Nanobiomedical Science, BK21 Plus NBM Global Research Center for Regenerative Medicine, Dankook University, Cheonan, Republic of Korea

Research Article

Nerve tissue engineering using blends of poly(3-hydroxyalkanoates) for peripheral nerve regeneration

The only types of polyhydroxyalkanoates (PHAs) that have been explored for use in nerve regeneration are poly(3-hydroxybutyrate), P(3HB), and poly(3-hydroxybutyrate-co-3-hydroxyhexanoate) (P(3HB-co-3HHx)). However, nerve regeneration induced by these PHAs is inferior to that of autologous nerve grafting. The aim of this work was to study novel PHA blends as resorbable biomaterials for the manufacture of nerve guidance conduits. PHA blend films with varying ratios of poly(3-hydroxyoctanoate)/poly(3-hydroxybutyrate) (P(3HO)/P(3HB)) were produced using the solvent-casting method. Neat films of P(3HO) and P(3HB), along with 25:75, 50:50, and 75:25 blend films of P(3HO)/P(3HB), were characterized with respect to chemical, material, and biological properties. On surface analysis, the blends exhibited higher values of roughness compared with the neat films. The differential scanning calorimetry characterization of the blends confirmed that P(3HO) and P(3HB) formed immiscible blends. FTIR and XRD analysis of the blends showed a decrease in crystallinity along with an increase of the proportion of P(3HO) . However, an increase in the stiffness of the blends was observed when the proportion of P(3HB) increased. Although all of the blends were biocompatible with NG108-15 neuronal cells, the 25:75 P(3HO)/P(3HB) blend showed significantly better support for growth and differentiation of these cells. The mechanical properties of PHA blends correspond to the reported properties of peripheral nerves. Therefore, they could serve as base material for the manufacture of nerve guidance conduits.

Keywords: Biocompatibility / *In vitro* test / Nerve regeneration / Neuronal cells / Polyhydroxyalkanoates

1 Introduction

Peripheral nerve injuries affect about 2.8% of trauma patients, many of who suffer life-long disability [1]. Peripheral nerves are able to repair when the injuries present a gap of less than 5 mm to bridge [2,3]. For injuries resulting in nerve damage with gaps of more than 5 mm, treatment is most commonly attempted using autologous nerve graft repair [4,5]. When nerve damage is even more extreme and gaps exceed 3 cm, allografts, vascularized nerve grafts, and nerve grafts without vessels are used [5]. Peripheral nerve repair using nerve autografts has several limitations including donor site morbidity, scar tissue invasion, scarcity of donor nerves, inadequate return of function, and aberrant regeneration [5, 6]. Currently, there are several clinically approved artificial nerve guidance conduits (NGCs) made from various biomaterials that have overcome some of the limitations of these nerve autografts. Conversely, NGCs made from synthetic materials can trigger immune responses, induce scar tissue and can release compounds that are detrimental to the nerve regeneration process [5].

During the past two decades a large variety of materials including nanostructured materials and biochemical factors have been explored in attempts to improve the quality of nerve

Correspondence: Dr. Ipsita Roy (royi@westminster.ac.uk), Applied Biotechnology Research Group, Department of Life Sciences, Faculty of Science and Technology, University of Westminster, 115 New Cavendish Street, W1W 6UW London, UK

Abbreviations: DSC, differential scanning calorimetry; **NGCs**, nerve guidance conduits; **PHAs**, polyhydroxyalkanoates; **PCL**, polycaprolactone; **PLCL**, poly(DL-lactide-ε-caprolactone); **P(3HB)**, poly(3-hydroxybutyrate); **P(3HB-co-3HHx)**, poly(3-hydroxybutyrate-co-3-hydroxyhexanoate); **P(3HO)**, poly(3-hydroxyoctanoate); **Rq**, root mean square roughness

conduits, and currently there are several commercial nerve conduits approved by US Food and Drug Administration (FDA) and Conformit Europe (CE) [2]. All of the models currently available take the form of a simple hollow tube with a single lumen. They possess no internal substructure, are made from either synthetic or natural materials, and are available in different designs and sizes [7]. The materials that have been used for their manufacture include poly(DL-lactide-ε-caprolactone), polyglycolic acid, PVA, collagen type I, and extracellular matrix. Furthermore, a large diversity of materials have been used experimentally to produce NGCs such as aliphatic polyesters, polylactic acids, poly-caprolactones, polyurethanes, silicones, collagens, glycoproteins, polypeptides, polyhydroxyalkanoates (PHAs), polysaccharides, proteins, and acellular or extracellular matrices.

PHAs possess great potential as materials for use in the manufacturing of NGCs to assist axonal regeneration. Their prominent properties such as controllable surface erosion, variability in material properties, lower acidity of degradation products, and longer stability compared to their synthetic counterparts are all of special interest in this field.

Currently, poly(3-hydroxybutyrate) (P(3HB)) and poly(3-hydroxybutyrate-*co*-3-hydroxyhexanoate) (P(3HB-*co*-3HHx)) are the only type of PHA that have been explored for their use in nerve regeneration. P(3HB) conduits have been shown to repair nerve gaps of 10 [8–12] and 40 mm [13, 14] in rat sciatic nerves and rabbit peroneal nerves, respectively. Hollow P(3HB-*co*-3HHx) conduits have also been used to bridge 10 mm defects in rat sciatic nerves [15]. Although these studies showed low level of inflammatory infiltration and suitable reabsorption time for nerve repair, the regeneration obtained was not statistically comparable with the regeneration obtained by using autologous nerve grafting.

The aim of this work was to investigate PHA blends as resorbable biomaterials for their use in the manufacture of NGCs. Mechanical, physical, and chemical properties of poly(3-hydroxyoctanoate) (P(3HO)), P(3HB), and their blends were characterized. The biocompatibility of these materials with NG108-15 neuronal cells was also studied. As P(3HO) displays mechanical properties similar to those of the peripheral nerve and P(3HB) have shown to be biocompatible to neuronal cells these PHAs were chosen for evaluation as improved materials for nerve tissue engineering.

2 Materials and methods

2.1 Production and extraction of P(3HO) and P(3HB)

Production, extraction, and purification of P(3HO) were performed as described previously [16]. The determination of lipopolysaccharides was also determined previously [16]. Production, extraction, and purification of P(3HB) were carried out as described previously [17].

2.2 Film preparation

Films of P(3HO), P(3HB), and three different blends of P(3HO)/P(3HB) were prepared using the solvent casting method. The PHAs were dissolved in chloroform in order to obtain a total polymer concentration of 5 w/v%. The P(3HO)/P(3HB) blends were prepared in ratios of 75:25, 50:50, and 25:75 by dissolving the required amounts of polymers in 10 mL of chloroform. After polymer dissolution, the solutions were homogenized by sonication and then cast in 6-cm glass petri dishes. The films were air dried for 2 wk and produced in triplicate to obtain a total of 15 films with varying thicknesses of 0.09–0.15 mm.

2.3 Scanning electron microscopy of the films

Surface topography of the films was analyzed using a FEI XL30 Field Emission Gun Scanning Electron Microscope (Eindhoven, the Netherlands). All the samples were previously sputter-coated with a 20 nm film of palladium using a Polaron E5000 sputter coater. The operating pressure of the sputter coating was 5×10^{-5} bar with a deposition current of 20 mA for a duration of 1 m and 30 s. The images were then recorded at different magnifications at 5kV using the FEI software.

2.4 Surface wettability of the films

The static contact angle of the films was carried out as described previously [18].

2.5 Profilometric surface analysis

The surface roughness of the films was analyzed using a Sony Proscan 1000 Laser Profilometer (Tokyo, Japan). The laser used was model 131 A, which has a measuring range of 400 μm, a resolution of 0.02 μm, and a maximum output of 10 mW. Scans of 0.5 mm^2 were obtained from each sample. Nine random coordinates were selected from each specimen in order to measure the root mean square roughness (Rq).

2.6 X-Ray diffraction analysis

Crystallization analysis of the films was performed using a Brüker D8 Advance diffractometer in flat plate geometry, using Ni-filtered Cu Ka, radiation. Data were collected from 10 to 40° with a primary beam slit size of 0.6 mm. A Brüker Lynx Eye silicon strip detector was used and a step size of 0.02° and a count time of 0.1 s per step.

2.7 Static tensile test of the films

Mechanical analysis of the films was conducted using a Perkin Elmer Dynamic Mechanical Analyser 7 (Norwalk, USA). The sample dimensions were 1.66–2.05 mm in width; 5–6 mm in length, and had a thickness of 0.05–0.18 mm. The load was set within a range of 1–6000 mN with a rate of 200 mN/min^{-1} at 24°C. The mechanical properties were determined using the software. This included analysis of Young's modulus, ultimate tensile strength, and elongation at break.

Engineering
in Life Sciences
www.els-journal.com

Eng. Life Sci. **2015**, *15*, 612–621

BIOtec
visions
www.biotecvisions.com

2.8 DSC

Thermal analysis of neat polymers and their blends was conducted using a differential scanning calorimetry (DSC) model TA Q2000 (TA Instruments, USA). Thermograms were acquired with the rate of temperature scan of $20°C \cdot min^{-1}$.

2.9 NG108-15 neuronal cell culture

NG108-15 neuronal cells were obtained from The European Collection of Cell Cultures (ECACC) and grown in DMEM under a humidified atmosphere of 5% CO_2 at 37°C. The DMEM was supplemented with 10% v/v FCS, 1% w/v glutamine, 1% w/v penicillin/streptomycin, and 0.5% w/v amphotericin B. Cells were only used in the experiments once they were 80–90% confluent. Cells were trypsinized and 3×10^4 cells were seeded directly onto the PHA film samples within 12-well plates in 3 mL of DMEM. The cultures were maintained for 4 days, with half of the medium being removed and replaced with fresh serum-free DMEM on day 2 to trigger experimental differentiation. NG-108-15 neuronal cells were used between passages 10 and 20.

2.10 Live/dead measurement of NG-108-15 neuronal cells

After growing cells for 4 days, the culture medium was removed and replaced with fresh serum-free DMEM containing 0.0015% w/v propidium iodide (Invitrogen) and 0.001% w/v Syto-9 (Invitrogen) at 37°C/5% CO_2 for 15 min. After washing with PBS (×3), the cells were imaged with an upright Zeiss LSM 510 confocal microscope. A helium–neon laser was used for the detection of propidium iodide (λex = 536 nm/λem = 617 nm) while an argon-ion laser was used for Syto 9 (λex = 494 nm/λem = 515 nm). Three fields of view were imaged containing 20–500 cells per sample, so as to express the data as a percentage of live versus dead cells ± SEM. Quantification of live and dead cells was performed using the software Image J.

2.11 Immunolabeling of NG108-15 neuronal cells

To assess the differentiation of neuronal cells, samples were immunolabeled using β III-tubulin as the primary antibody and with Alexa Fluor 488 goat anti-mouse IgG as the secondary antibody. Sample films containing cultures of NG108-15 neuronal cells previously washed with PBS (×3), were fixed with 4% v/v paraformaldehyde for 20 min, then permeabilized with 0.1% v/v Triton X-100 for 20 min, before being washed with PBS (×3). Unreactive binding sites were blocked with 3% w/v BSA with the cells being incubated overnight with mouse anti β III-tubulin antibody (1:1000) (Promega, USA) diluted in 1% BSA at 4°C. Cells were then washed three times with PBS before being incubated with Alexa Fluor 488 goat anti-mouse IgG antibodies (1:200 in 1% BSA) (Sigma Aldrich) for 90 min. After washing the cells once with PBS, 4′,6-diamidino-2-phenylindole dihy-

drochloride (Sigma Aldrich) (1:500 dilution in PBS) was added to label nuclei. Cells were then immersed for 15 min at room temperature before being washed again with PBS (×3). Cells were then imaged using an upright Zeiss LSM 510 confocal microscope. Nuclei were visualized by two photon excitation using a Ti:sapphire laser (716 nm) for 4′,6-diamidino-2-phenylindole dihydrochloride (λex = 358 nm/λem = 461 nm). For imaging the neuronal cell body and neurites of NG108-15 cells, a helium–neon laser (543 nm) was used to detect the Alexa Fluor 488 goat anti-mouse IgG (λex = 589 nm/λem = 615 nm). The differentiated cells were then counted using ImageJ software, identified as neuronal cells expressing neurites.

2.12 Statistical analysis

Statistical analysis was conducted using Graph Pad Prism 6 software. Shapiro–Wilk and Bartlett's tests were performed to verify data normality and homogeneity, respectively. To analyze the differences between groups, a one-way ANOVA test ($p < 0.05$) was conducted followed by Turkey's post-test ($p < 0.05$). Data are reported as means ± SEM.

3 Results

3.1 Scanning electron microscopy of the PHA films

Scanning electron microscopy images of the films were obtained in order to compare their surface morphology. The P(3HO) film (Fig. 1A) displayed the presence of pores with sizes ranging from 0.1 to 5 μm. The 75:25 (Fig. 1B) and 25:75 (Fig. 1D) blends presented smaller and less abundant pores (0.1–3 μm) compared to the P(3HO) film. Conversely, pores were not detected in the 50:50 blend (Fig. 1C), which showed protrusions uniformly distributed on the surface. The P(3HB) film (Fig. 1E) displayed the smoothest and most homogenous surface without the presence of pores. It was observed that the presence of P(3HO) in the blends increased the porosity compared with the neat P(3HB).

3.2 Profilometric surface analysis

The Rq of the films was determined using a laser profilometer. The roughness of P(3HO) and P(3HB) films was significantly different (3.69 ± 0.20 nm vs. 2.60 ± 0.09 nm, $p < 0.05$). Although the P(3HO) film was the most porous, its roughness (3.69 ± 0.20 nm) was not significantly different to the roughness of the 75:25, 50:50, and 25:75 blends (4.00 ± 0.15 nm, 4.23 ± 0.37 nm, 4.16 ± 0.25 nm, $p > 0.05$). On the other hand, statistical analysis showed that the roughness of P(3HB) (2.60 ± 0.09 nm) was significantly different to that of the blends 25:75, 50:50, and 75:25 (4.00 ± 0.15 nm, 4.23 ± 0.37 nm, 4.16 ± 0.25 nm, $p < 0.05$). As expected, the neat P(3HB) film presented the lowest value of roughness, which correlates with its surface having the smoothest appearance of all the films, as can be observed in the scanning electron microscopy analysis (Fig. 1F).
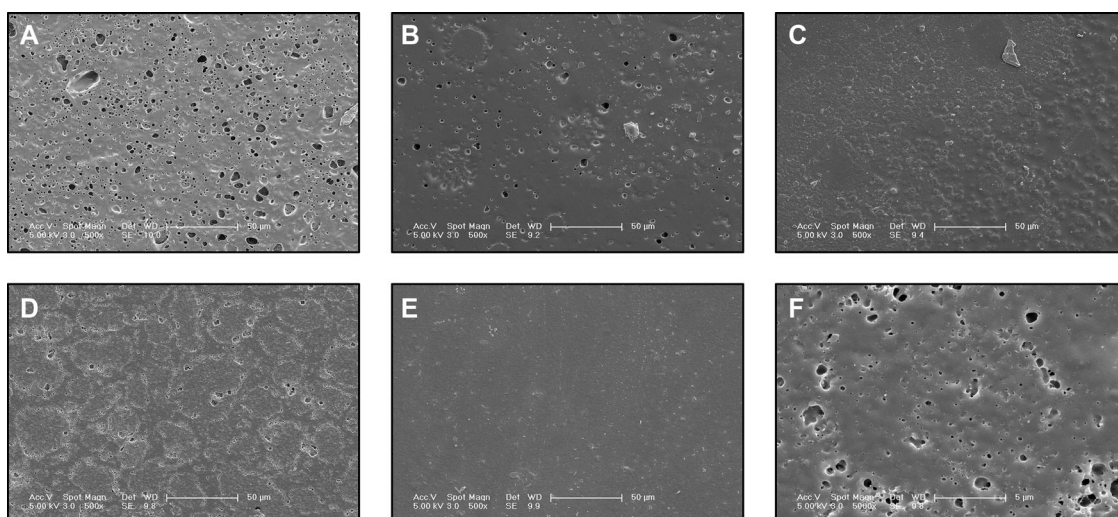
Engineering
in Life Sciences

www.els-journal.com

Eng. Life Sci. **2015**, *15*, 612–621

BIO tec
visions

www.biotecvisions.com

Figure 1. Characterization of the surface topography of P(3HO)/P(3HB) films by scanning electron microscopy analysis. (A) P(3HO); (B) 75:25; (C) 50:50; (D) 25:75; (E) P(3HB); and (F) 25:75 blend at 500×. Films P(3HO) (A), 75:25 (B), and 25:75 (D) showed porous topography whereas the P(3HB) (E) presented smooth surface. The surface of blend 50:50 (C) presented protrusions uniformly without pores. (F) Higher magnification (5000×) of the 25:75 blend shows its porous structure.

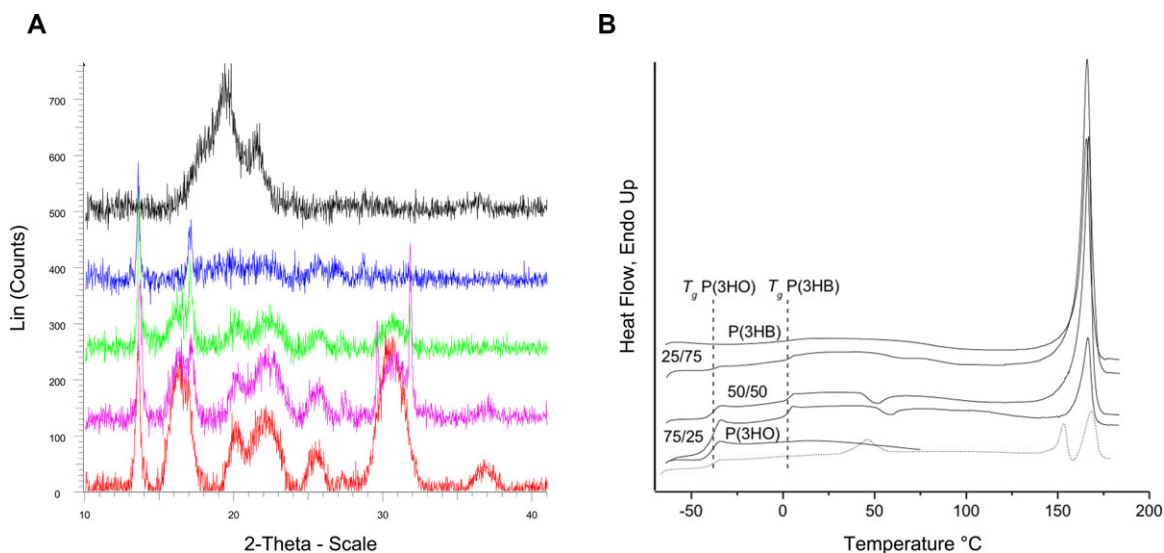**Figure 2.** ■P(3HO); ■75:25 P(3HO)/P(3HB), ■50:50 P(3HO)/P(3HB), ■25:75 P(3HO)/P(3HB), ■P(3HB). (A) XRD spectra of P(3HO)/P(3HB) films showing crystalline (sharp peaks) and amorphous (broad peaks) phases of the polymers. As the content of P(3HB) increased in the blend, the number the peaks increased too. (B) DSC thermograms of neat polymers and their blends. Dotted line: representative thermogram of the first heating scan of aged 75:25 blend. Solid lines: thermograms of the second heating run.

3.3 X-Ray diffraction analysis

The solvent-casted films were characterized by wide-angle X-ray diffraction spectroscopy. The neat P(3HB) film exhibited two intense peaks at 2θ values of 13.5° and 16.4° (Fig. 2A). The peak positions correspond to the reported values in previous studies of P(3HB) [19,20] crystalline structure where they were assigned to the (020) and (110) planes of the orthorhombic unit cell. Moreover, a series of peaks was observed in 2θ range between 18° and 34°. These peaks are most likely attributed to the crystalline lattice planes of (021), (120), (111) and (101). In contrast to neat

P(3HB), the diffraction pattern of P(3HO) was characterized by the presence of a broad amorphous halo located around 2θ = 20°. However, in the P(3HO) diffractogram the amorphous halo was superposed with a series of diffraction peaks around 17°, 19°, and 21°. Thus a significant fraction of semicrystalline P(3HO) was in amorphous phase. X-ray diffractograms of all the blends showed intense peaks of P(3HB) (020) and (110) planes indicating that P(3HB) crystallized in the presence of P(3HO) even when the concentration of P(3HO) was 75%. However, peaks corresponding to P(3HO) crystallites were not detected in the diffractograms of the blends. Also, the weak amorphous halo

Engineering
in Life Sciences

www.els-journal.com

Eng. Life Sci. **2015**, *15*, 612–621

BIOtec visions
www.biotecvisions.com

was observed only in the 75:25 blend while other blend compositions did not show P(3HO) amorphous phase. Comparing the spectrum of the pure P(3HB) with those of the blends, it was seen that peak positions corresponding to P(3HB) were constant. This indicated that the P(3HB) unit cell did not change in the blends.

3.4 DSC

A representative thermogram of aged P(3HO)/P(3HB) blends (Fig. 2B) shows the presence of two endothermic events with peak temperatures around 50°C and above 150°C corresponding to the melting temperatures (T_m) of P(3HO) and P(3HB), respectively. After erasing the thermal history and material cooling at 20°C/min, neither material including neat P(3HO) showed the lower temperature melting event. Thus such cooling conditions do not allow crystallization of P(3HO). The blending of these two polymers did not have any effect on the T_m of P(3HB). These PHAs have distinctive glass transitions (T_g) namely −39 and 2°C for P(3HO) and P(3HB), respectively. Blends of these polymers were characterized by the presence of two glass transition events. Similar to melting, positions of both glass transitions were not affected by the presence of the second polymer. Interestingly, cold crystallization was observed for the blends with high P(3HO) content (50:50 and 75:25) as shown by the relatively narrow exothermal peaks between 40 and 70°C. In contrast, the cold crystallization of neat P(3HB) and the 25:75 blend were barely detectable, they manifested as slight depreciation of the baseline at temperatures above 60°C lasting until the endothermic melting of the P(3HB) crystals. It appears that P(3HB) crystallizes to the same degree as P(3HB) in blends with P(3HO) content up to 50%. Specific enthalpy of fusion (ΔH_f) had slight fluctuations for P(3HB), 25:75, 50:50 blends, namely 73.4, 74.4, 71.6 J per gram of P(3HB), respectively. However, it significantly decreased to 28.8 J per gram of P(3HB) for the 75:25 blend.

3.5 Surface wettability

Surface wettability of the PHA films was analyzed by measuring the water contact angle. Wettability describes how easy a fluid spreads or adheres across a solid surface. A high contact angle signifies low wettability whereas a low contact angle means high wettability. When the contact angle between distilled water and the surface of a solid substrate is less than 90°, the material is said to be hydrophilic or wet. When the angle is greater than 90°, the material is called hydrophobic or water repellent [21]. The water contact angle of the P(3HO)/P(3HB) films decreased as the content of P(3HO) decreased ((P(3HO), 103.56 ± 0.95; 75:25, 94.41 ± 1.16; 50:50, 84.40 ± 0.70; 25:75, 77.36 ± 0.81; P(3HB), 69.69 ± 1.63) (Fig. 3). This is due to the long aliphatic chains present in P(3HO) that constitute its hydrophobic character. The statistical analyses showed that the differences in water contact angle between all the films P(3HO)/P(3HB) were significant (*p*-value < 0.05). As the water contact angle of both the P(3HO) and the 75:25 P(3HO)/P(3HB) films were greater than 90°, they are considered to be hydrophobic in nature. By contrast, the water contact angles of the 50:50, 25:75 blend films, and the P(3HB) films were less than 90° and are therefore hydrophilic.
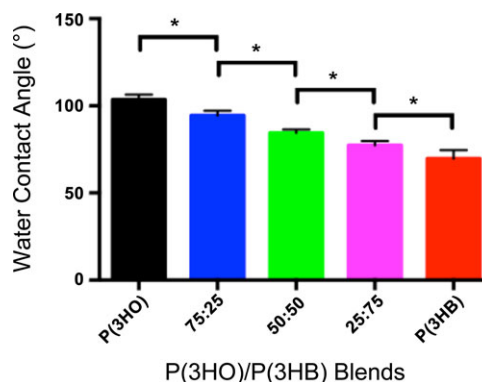

Figure 3. Static water contact angle of P(3HO)/P(3HB) films. The water contact increased as the content of P(3HO) increased in the blend. The water contact angle was significantly different for all the blends (mean ± SEM, $n = 9$ independent experiments, *$p <$ 0.05).

Table 1. Mechanical analysis of the P(3HO)/P(3HB) films

P(3HO)/ P(3HB) film	E (MPa)	Tensile strength (MPa)	Percentage strain
100:0	1.88 ± 0.12	4.91 ± 0.33	286.42 ± 18.48
75:25	1.25 ± 0.18	0.71 ± 0.08	73.82 ± 18.08
50:50	21.83 ± 0.95	2.17 ± 0.92	94.18 ± 3.52
25:75	143.40 ± 2.16	17.80 ± 0.80	41.30 ± 1.73
0:100	1160 ± 185.87	28.60 ± 1.76	9.6 ± 2.62

3.6 Static tensile test of the films

Mechanical properties of the films were measured through the static tensile test. Young's Modulus (E values), tensile strength, and elongation at break of the different films are shown in Table 1. Young's modulus, a measure of the stiffness of materials, was determined by calculating the slope of the linear region of the stress–strain curve. The tensile strength is the maximum load that a material can sustain during the test, whereas the elongation at break is the ratio between the final length before breakage and the initial length of the specimen. The E values of the blends and P(3HO) were significantly different to P(3HB) E value (*p*-value < 0.05). The tensile strength values were all significantly different when compared against each other excepting P(3HO) and the blend 75:25 of which difference was not significant. All the values of percentage strain were significantly different from P(3HO) percentage strain (*p*-value < 0.05). When the percentage strain values of the blends were compared against each other the only significant difference was found between the blends 50:50 and 25:75. When the percentage strain of P(3HB) was compared with the blends the only significant difference found was when compared with the blend 50:50. Stiffness of the blends increased when increasing the content of P(3HB) excepting for the 75:25 P(3HO)/P(3HB) blend. In the other hand, the pliability of the blends decreased when increasing the P(3HB) content.
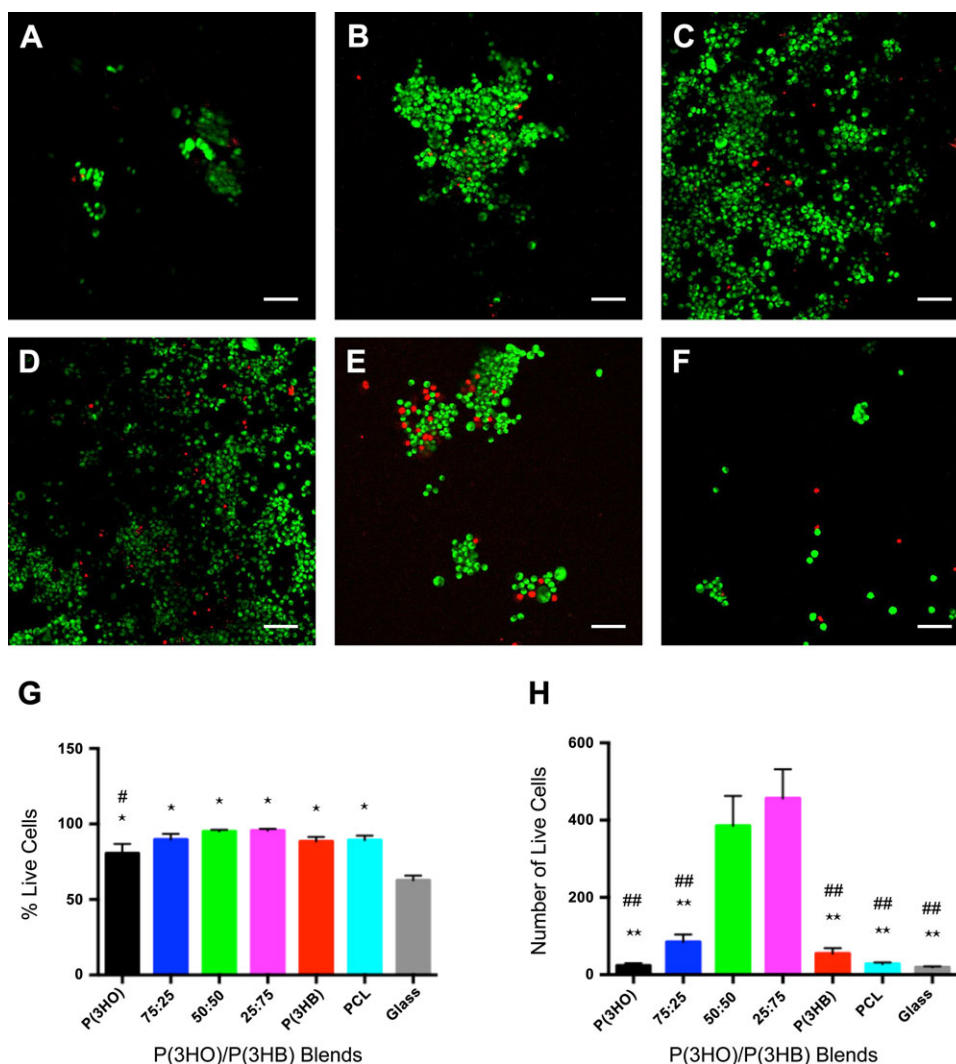
Engineering
in Life Sciences

www.els-journal.com

Eng. Life Sci. **2015**, *15*, 612–621

BIOtec visions

www.biotecvisions.com

Figure 4. Confocal micrographs of NG108-15 neuronal cells labeled with propidium iodide (red) and Syto-9 (green) after 4 days in culture on P(3HO)/P(3HB) films and PCL. (A) P(3HO); (B) 75:25; (C) 50:50; (D) 25:75; (E) P(3HB); and (F) PCL. Cell growth was randomly oriented on each of the flat substrates. (G) Live/dead analysis of neuronal cells on the P(3HO)/P(3HB) blends, PCL, and glass (control). Percentage of live neuronal cells on all the blends and PLC was higher in comparison to glass (control) (mean ± SEM, $n = 9$ independent experiments; *$p < 0.05$). Percentage of live neuronal cells on P(3HO) was lower compared to the 25:75 blend (mean ± SEM, $n = 9$ independent experiments; #$p < 0.05$). (H) Number of live cells on the P(3HO)/P(3HB) blends, PCL, and glass (control). The number of live cells on P(3HO), 75:25, P(3HB), PCL, and glass decreased in comparison to the 50:50 and 25:75 blends (mean ± SEM, $n = 9$ independent experiments; **$p < 0.05$ compared to 50:50, ##$p < 0.05$ compared to 25:75).

3.7 Live/dead measurement of NG-108-15 neuronal cells

A live/dead cell measurement was conducted in order to compare the attachment and survival of NG-108-15 neuronal cells on the P(3HO)/P(3HB) films using polycaprolactone (PCL) and glass as controls. In Fig. 4, representative confocal images of the cells grown in the different substrates can be seen. Images (C) and (D) correspond to the 50:50 and 25:75 blends, respectively, and displayed the highest density of cells compared with the other images.

The percentage of live cells grown on P(3HO), 75:25, 50:50, 25:75, and P(3HB) films was 80.54 ± 6.26%, 89.73 ± 3.68%, 95.12 ± 1.02%, 95.59 ± 1.23%, 88.40 ± 2.99%, and on PCL was 89.29 ± 3.06%. This was higher when compared with glass substrate (62.68 ± 3.15%) (Fig. 4G). Statistical analysis showed that the difference in the percentage of live cells was significant for all the substrates including PCL when compared with that of glass ($p < 0.05$). The difference in the percentage of live

cells between the 75:25, 50:50, 25:75 P(3HO)/P(3HB), and PCL substrates was not significant ($p > 0.05$). The only significant difference in the percentage of live cells found between the substrates was when the P(3HB) (80.54 ± 6.26%) and the 25:75 blend (95.59 ± 1.23%) were compared ($p < 0.05$). Hence, the percentage of live cells obtained using the P(3HO)/P(3HB) 25:75 film was significantly higher than that obtained with P(3HB).

In Fig. 4H, the average number of cells in the different substrates is shown. The 50:50 and 25:75 blends were associated with the highest number of adhered neuronal cells per view (385.11 ± 77.69 cells and 456.00 ± 75.67 cells, respectively). No significant differences were found in the number of adhered neuronal cells on 50:50 and 25:75 polymer blends. Statistical analysis demonstrated that the number of cells on the 50:50 and 25:75 blends was significantly higher than the other substrates, including PCL and glass. The difference in the number of live cells found between the P(3HO), 75:25, P(3HB), PCL, and glass substrates was not significant (23.78 ± 5.96, 84.56 ± 19.92, 54.22 ± 14.04, 27.78 ± 4.07, 19.00 ± 2.52).
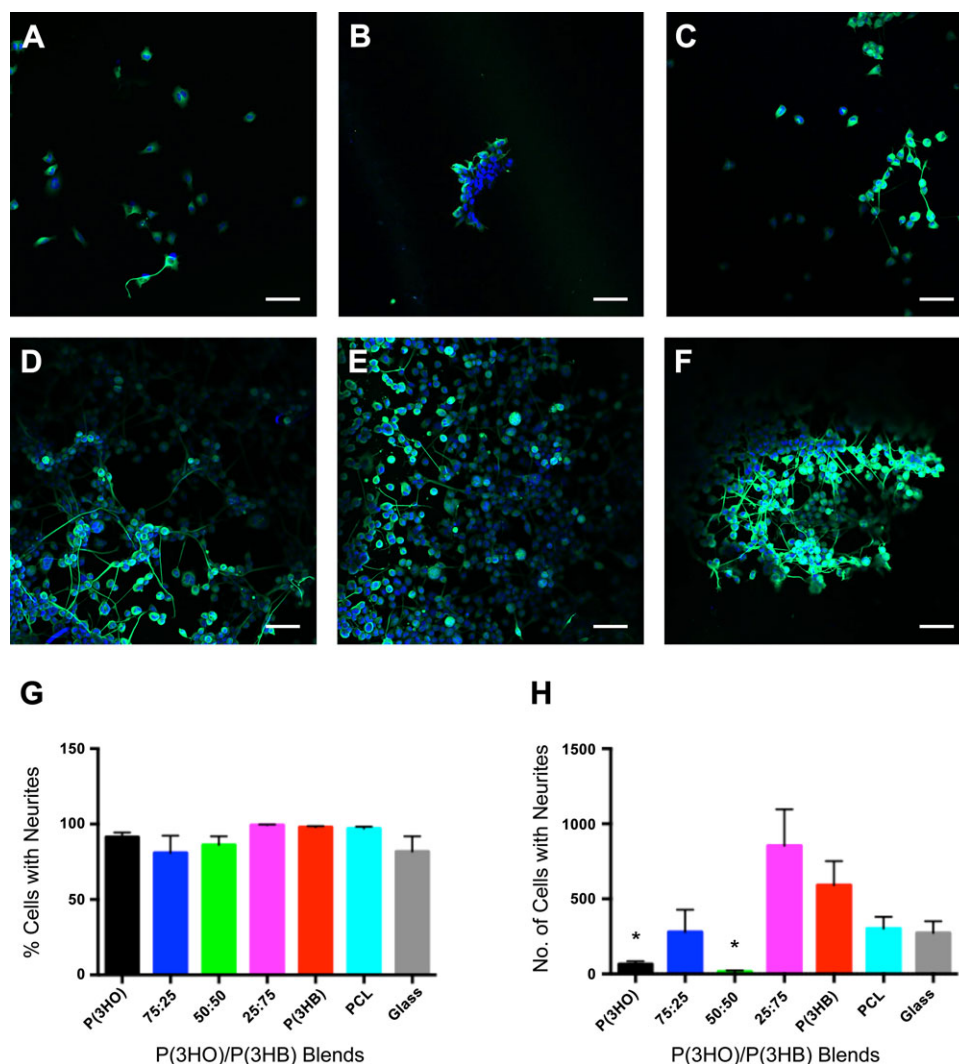
Figure 5. Confocal micrographs of NG108-15 neuronal cells immunolabeled for beta-III tubulin after 4 days in culture on P(3HO)/P(3HB) films and PCL. (A) P(3HO); (B) 75:25; (C) 50:50; (D) 25:75; and (E) P(3HB); and (F) PCL. Neurite outgrowth was randomly oriented on each of the flat substrates. (G) Percentage of cell with neurites on the P(3HO)/P(3HB) blends, PCL and glass (control). Percentage of neurites on all the blends, PLC, and glass was similar (mean $\pm$ SEM, $n = 6$ independent experiments, $p < 0.05$). (H) Number of cells with neurites on the P(3HO)/P(3HB) blends, PCL, and glass (control). The number of cell with neurites on P(3HO) and 50:50 was lower in comparison to 25:75 blend (mean $\pm$ SEM, $n = 6$ independent experiments; *$p < 0.05$).

3.8 Neurite outgrowth assessment

NG108-15 neuronal cells were immunolabeled with the anti-β III-tubulin antibody to assess neurite outgrowth on the substrates. The protein β-III-tubulin is considered a neuron-specific marker as this molecule is expressed in neuronal cell bodies, dendrites, axons, and axonal terminations. Therefore, this protein is widely used as an indicator of neuronal cell differentiation. Figure 5A–F shows the confocal images of neuronal cells grown on each of the substrates, where neurite outgrowth can clearly be observed. However, two important characteristics of neuronal cells grown on the 25:75 blend, P(3HB) and PCL films were both the presence of several neurite-bearing neurons and the appearance of longer neurites compared with those cells grown on the P(3HO), 25:75, and 50:50 P(3HO)/P(3HB) blends.

Figure 5G shows the percentage of cells containing neurites on each substrate. Statistical analysis showed no significant difference in the percentage of cells with neurites for the P(3HO), 25:75, 50:50, 25:75, P(3HB) (91.42 $\pm$ 2.99; 80.90 $\pm$ 11.39; 86.15 $\pm$ 5.76; 99.30 $\pm$ 0.40; 97.98 $\pm$ 0.73), PCL (97.00 $\pm$ 1.30), and glass

(81.85 $\pm$ 9.64), ($p < 0.05$). Figure 5H, shows the number of cells with neurites in the different substrates. There was no significant difference in the number of cells with neurites on PCL (303.00 $\pm$ 77.94), glass (273.00 $\pm$ 77.94), 75:25 (280.00 $\pm$ 147.31), 25:75 (854.00 $\pm$ 243.02), and P(3HB) (591.00 $\pm$ 159.34) ($p < 0.05$). However, the number of cells with neurites on 25:75 blend was significantly higher compared to the P(3HO) and 50:50 blends ($p < 0.05$).

4 Discussion

The presence of two glass transitions and melting events in P(3HO)/P(3HB) blends, which occurs at the same temperatures as neat polymers (Fig. 2B) indicates that the PHAs used in this study were immiscible in both amorphous and crystalline phase. The independence of specific enthalpy of fusion of P(3HB) for blends with P(3HO) content up to 50% indicated that P(3HB) crystallizes as separate phase in the presence of P(3HO). Although the aged blends show melting of P(3HO) crystals, the

Engineering
in Life Sciences
www.els-journal.com
Eng. Life Sci. **2015**, *15*, 612–621
BIOtec visions
www.biotecvisions.com

crystallization was slower than P(3HB) and occurred when crystallization of main part of P(3HB) was complete. Apparently, the presence of medium chain length PHA, a polymer with lower glass transition temperature, accelerates the kinetics of P(3HB) crystallization. This was observed in the P(3HB) non-isothermal crystallization, which was characterized by cold crystallization for blends containing up to 50% of P(3HO). Such influence of medium chain length PHA on the crystallization of P(3HB) could be due to the increase of polymer chain mobility in the system containing polymer in rubbery state. However, in the 75:25 blend crystallization of P(3HB) was significantly suppressed.

Crystallization of P(3HB) was also confirmed by XRD. Although intensities of the peaks in the diffractograms of P(3HO)/P(3HB) blends decreased with the increase of P(3HO) content their positions were essentially the same as the peaks on the diffractogram of P(3HB). The peaks characteristic for P(3HO) were not detectable even in the blend with the highest P(3HO) content. That might imply that P(3HO) cocrystallized with P(3HB). However, considering that DSC experiment showed two separate melting events exactly matching the melting temperatures of the neat polymers, it is unlikely that these two PHAs could cocrystallize. One might suggest that crystallites of P(3HO) did not develop sufficiently in the blends in order to be detectable in XRD.

The surface of the P(3HB) film was found to be smooth whereas the surface of the P(3HO) film was porous. The smooth surface observed in P(3HB) film was similar to that characterized by Wang et al., where the degradation of P(3HB) by polyhydroxybutyrate depolymerase was investigated [22]. Conversely, this smooth appearance contrasts with the porous morphology of a P(3HB) film characterized by Kai et al. [23] in their study of P(3HB-co-3HHx)/P(3HB) blends. Although the surfaces of P(3HO) films have shown to be smooth and nonporous in previous studies [16, 18] it is worth noting that there is a lack of information available relating to the characterization of P(3HO) for comparison.

The smooth appearance shown in the scanning electron microscopy images of P(3HB) film was in accordance with the profilometric analysis in which this film presented the lowest root square mean roughness. The higher Rq values of P(3HO) compared to that of P(3HB) might be attributed to its porous surface. The higher Rq values of the 75:25, 50:50, and 25:75 P(3HO)/P(3HB) blend films compared to the P(3HO) and P(3HB) film corroborated the phase separation process detected in the blend films by DSC analysis. Furthermore, it has been shown that when smooth blend films are produced using a wide compositional range, the polymers have a high level of compatibility [24]. Most of the Rq values of P(3HO) and P(3HB) films found in the available literature have been obtained using atomic force microscopy and not by profilometric analysis. As it has been found that there is a discrepancy in the resultant Rq values between these two techniques, comparisons with these values were not feasible [25].

It has been shown that the forces affecting the wettability in a solid substrate are the surface tension of the substrate, the surface tension of the liquid, and the interfacial tension. The hydrophobicity of blend materials can change due to compositional variations and the arrangement of polymer molecules in surface layers. When polymer films are formed from polymer solutions the solution interface is exposed to the hydrophobic air environment. Thus, polymeric molecules in the surface may reorientate their hydrophobic groups toward the surface of the material, resulting in a less wettable surface. The neat P(3HO) film was the most hydrophobic one. This polymer has a longer aliphatic chain per monomer unit with four more methyl groups compared with P(3HB). These methyl groups may have rotated toward the hydrophobic interface through chain rotation. This orientation is more favourable energetically and decreases the surface free energy [26]. Therefore, the observed decrease in the wettability of the films as the P(3HO) content increased demonstrates the higher number of hydrophobic chains present in the films.

The Young's modulus, tensile strength, and elongation at break values obtained for the P(3HO) and 50:50 blend differed slightly from the mechanical properties determined for similar films previously examined [18]. The higher Young's modulus values obtained in this study for the P(3HO) and 50:50 blend could be the result of variations in the molecular weight of the polymers. It has been shown that lower molecular weights of the same polymer increase Young's modulus and tensile strength values [27]. Therefore, these results suggest that the molecular weight of the P(3HO) used in this study could be higher than that used by Basnett et al. It is well known that cultivation conditions can affect the molecular weight of PHAs. Tomizawa et al. and Agus et al. showed that the molecular weight of P(3HB) decreased with an increase in culture time and temperature [28, 29]. The mechanical properties of P(3HB) obtained in this study agreed with values obtained in similar studies [30]. The Young's modulus of the 75:25 P(3HO)/P(3HB) blend (1.25 ± 0.18 MPa) and the tensile strength (0.71 ± 0.08 MPa) were the most similar to that of peripheral nerves in rats (0.58 ± 0.16 MPa and 1.4 ± 0.29 MPa, respectively). However, the 25:75 P(3HO)/P(3HB) blend displayed similar percentage of strain (41.30 ± 1.73%) to that of peripheral nerve in the same study (48 ± 11.7%) [31]. It is important to notice that the mechanical properties of nerves vary depending on the nature of the peripheral nerve being considered and the species from which the nerve was taken. In another study, the tensile strength and percentage of strain of rabbit peroneal nerve were 11.7 ± 0.7 MPa and 38.5 ± 2%, respectively, which are similar to those of the 25:75 P(3HO)/P(3HB) blend (17.80 ± 0.80 MPa and 41.30 ± 1.73%, respectively) [32]. Therefore, PHA-based blend could provide the appropriate resistance and elasticity that NGCs require for adequate flexibility at the site of implantation.

The superior biocompatibility displayed in the 50:50 and 25:75 P(3HO)/P(3HB) blends could be attributed to the higher roughness values featured in these films and their lower hydrophobicity compared to P(3HO) and 75:25 P(3HO)/P(3HB) films. It is well known that cell attachment is enhanced by the roughness, porosity, and hydrophilicity. However, in the neurite outgrowth test, the 50:50 blend presented a very low number of cells with neurites compared with the 25:75 P(3HO)/P(3HB) blend, which supported the highest number of cells containing neurites. Therefore, these findings indicate that the 25:75 blend support significantly better the growth and differentiation of NG108-15 neuronal cells. Biocompatibility studies of NG108-15 neuronal cells with PHAs have only been performed on P(3HB) substrates. P(3HB) has demonstrated high

biocompatibility not only with NG108-15 neuronal cells [32] but also with neuronal cells in animal models [8–14]. Armstrong et al. have used NGC made from P(3HB) as a substrate to investigate the effect of Schwann cells on neurite outgrowth NG108-15 neuronal cells [33].

The growth of NG108-15 neuronal cells was characterized by their irregular distribution in various layers on all substrates showing a random migration of cells. Neuronal migration is highly dependent on the expression of cell adhesion proteins, which can also be involved in neuronal differentiation. In neuronal cells, including NG108-15, different families of proteins regulate cell–cell and cell–substrate interactions: the Efh family, α-β-hydrolase fold family, and three families of CAMs; the Ig superfamily CAMs, cadherins, and integrins [34–39]. It has been shown that cell adhesion to polymeric surfaces such as PHA films is mediated mainly by integrins through the interactions between proteins and the polymers [40, 41]. Proteins coming from the serum, the surrounding medium or those produced by the cells could be adsorbed into the surface of the films and recognized by integrins through the Arg-Gly-Asp (L-arginine-glycine-L-aspartic acid) sequence which is present in a considerable number of proteins.

In summary, although all of the P(3HO)/P(3HB) blends and P(3HO) were able to support neuronal growth, the 25:75 P(3HO)/P(3HB) and P(3HB) films supported better neurite extension. Although both 75:25 P(3HO)/P(3HB) and 25:75 P(3HO)/P(3HB) blends presented suitable tensile strength and percentage of strain for their application in peripheral nerve repair, the 25:75 P(3HO)/P(3HB) blend displayed the highest biocompatibility among all the substrates.

Practical application

The standard treatment for peripheral nerve repair is the nerve autograft, which has several limitations including donor site morbidity, scar tissue invasion, scarcity of donor nerves, inadequate return of function, and aberrant regeneration. Although artificial NGCs made from various biomaterials have been clinically approved, they have not been able to overcome these limitations and can induce scar tissue and release compounds that are detrimental to the nerve regeneration process. Therefore, in this study, blends of PHAs, that have not been used before in nerve tissue engineering were analyzed for their potential use in the manufacture of multichannel and electrospun NGCs. PHAs displayed properties that could overcome some of the limitations of the available NGCs such as controllable surface erosion, lower acidity of their degradation products, and longer-lasting stability compared to their synthetic counterparts.

The authors have declared no conflict of interest.

5 References

[1] Midha, R., Emerging techniques for nerve repair: Nerve transfers and nerve guidance tubes. *Clin. Neurosurg.* 2006, *53*, 185–190.

[2] Jiang, X., Shawn, H. L., Mao, H-Q., Chew, S. Y., Current applications and future perspectives of artificial nerve conduits. *Exp. Neurol.* 2010, *223*, 86–101.

[3] Schmidt, C. E., Leach, J. B., Neural tissue engineering: Strategies for repair and regeneration. *Annu. Rev. Biomed. Eng.* 2003, *5*, 293–347.

[4] De Ruiter, G. C. W., Malessy, M. J. A., Yaszemski, M. J., Windebank, A. J. et al., Designing ideal conduits for peripheral nerve repair. *Neurosurg. Focus* 2009, *26*, 1–14.

[5] Babu, P., Behl, A., Chakravarty, B., Bhandari, P. S. et al., Entubulation techniques in peripheral nerve repair. *Ind. J. Neurotrauma* 2008, *5*, 15–20.

[6] Huang, W., Begum, R., Barber, T., Ibba, V. et al., Regenerative potential of silk conduits in repair of peripheral nerve injury in adult rats. *Biomaterials* 2012, *33*, 59–71.

[7] Bell, J. H. A., Haycock, J. W., Next generation nerve guides—materials, fabrication, growth factors and cell delivery. *Tissue Eng.* 2012, *18*, 116–128.

[8] Hart, A. M., Wiberg, M., Terenghi, G., Exogenous leukaemia inhibitory factor enhances nerve regeneration after late secondary repair using a bioartificial nerve conduit. *Br. J. Plast. Surg.* 2003, *56*, 444–450.

[9] Hazari, A., Wiberg, M., Johansson-Rudén, G., Green, C. et al., A resorbable nerve conduit as an alternative to nerve autograft in nerve gap repair. *Br. J. Plast. Surg.* 1999, *52*, 653–657.

[10] Mosahebi, A., Woodward, B., Wiberg, M., Martin, R. et al., Retroviral labelling of Schwann cells: In vitro characterization and in vivo transplantation to improve peripheral nerve regeneration. *Glia* 2001, *34*, 8–17.

[11] Mosahebi, A., Fuller, P., Wiberg, M., Terenghi, G., Effect of allogeneic Schwann cell transplantation on peripheral nerve regeneration. *Exp. Neurol.* 2002, *173*, 213–223.

[12] Mosahebi, A., Wiberg, M., Terenghi, G., Addition of fibronectin to alginate matrix improves peripheral nerve regeneration in tissue-engineered conduits. *Tissue Eng.* 2003, *9*, 209–218.

[13] Mohanna, P. N., Terenghi, G., Wiberg, M., Composite PHB-GGF conduit for long nerve gap repair: A long-term evaluation. *Scand. J. Plast. Reconstr. Surg. Hand Surg.* 2005, *39*, 129–137.

[14] Young, R. C., Wiberg, M., Terenghi, G., Poly-3-hydroxybutyrate (PHB): A resorbable conduit for long-gap repair in peripheral nerves. *Br. J. Plast. Surg.* 2002, *55*, 235–240.

[15] Bian, Y-Z., Wang, Y., Aibaidoula, G., Chen, G-Q. et al., Evaluation of poly(3-hydroxybutyrate-co-3-hydroxyhexanoate)

conduits for peripheral nerve regeneration. *Biomaterials* 2009, *30*, 217–225.

[16] Rai, R., Yunos, D. M., Boccaccini, A. R., Knowles, J. C. et al., Poly-3-hydroxyoctanoate P(3HO), a medium chain length polyhydroxyalkanoate homopolymer from Pseudomonas mendocina. *Biomacromolecules* 2011, *12*, 2126–2136.

[17] Valappil, S.P., Peiris, D., Langley, G.J., Herniman, J. M. et al., Polyhydroxyalkanoate (PHA) biosynthesis from structurally unrelated carbon sources by a newly characterized *Bacillus* spp. *J. Biotechnol.* 2007, *127*, 475–487.

[18] Basnett, P., Ching, K. Y., Stolz, M., Knowles, J. C., Novel poly(3-hydroxyoctanoate)/poly(3-hydroxybutyrate) blends for medical applications. *React. Funct. Polym.* 2013, *73*, 1340–1348.

[19] Capitan, M. J., Rueda, D. R., Ezquerra, T.A., Inhibition of the crystallization in nanofilms of poly(3-hydroxybutyrate). *Macromolecules* 2004, *37*, 5653–5659.

[20] Yokouchi, M., Chatani, Y., Tadokoro, H., Teranishi, K. et al., Structural studies of polyesters: Molecular and crystal structures of optically active and racemic poly (β-hydroxybutyrate). *Polymer* 1973, *14*, 233–288.

[21] Förch, R., Schönherr, H., Jenkins, A. T. A., Appendix C: Contact angle goniometry, in: Förch, R., Schönherr, H., Jenkins, A. T. A. (Eds.), *Surface Design: Applications in Bioscience and Nanotechnology*, Wiley-VCH Verlag GmbH & Co. KGaA, Weinheim 2009, pp. 471

[22] Wang, Y., Li, F., Wang, Z.-Y., Liu, D.-B. et al., Purification and properties of an extracellular polyhydroxybutyrate depolymerase from *Pseudomonas mendocina* DSWY0601. *Chem. Res. Chin. Univ.* 2012, *28*, 459–464.

[23] Kai, Z., Ying, D., Guo-Qiang, C., Effects of surface morphology on the biocompatibility of polyhydroxyalkanoates. *Biochem. Eng. J.* 2003, *16*, 115–123.

[24] Gutmann, J. S., Müller-Buschbaum, P., Schubert, D. W., Stribeck, N. et al., Roughness correlations in ultra-thin polymer blend films. *Physica B Condens. Matter* 2000, *283*, 40–44.

[25] Poon, C. Y., Bhushan, B., Comparison of surface roughness measurements by stylus profiler, AFM and non-contact optical profiler. *Wear* 1995, *190*, 76–88.

[26] Menzies, K. L., Jones, L., The impact of contact angle on the biocompatibility of biomaterials. *Optom. Vis. Sci.* 2010, *87*, 387–99.

[27] Al-Nasassrah M. A., Podczeck, F., Newton, J. M., The effect of an increase in chain length on the mechanical properties of polyethylene glycols. *Eur. J. Pharm. Biopharm.* 1998, *46*, 31–38.

[28] Tomizawa S., Hyakutake, M., Saito, Y., Agus, J. et al., Molecular weight change of polyhydroxyalkanoate (PHA) caused by the PhaC subunit of PHA synthase from Bacillus cereus YB-4 in recombinant *Escherichia coli*. Biomacromolecules 2011, *12*, 2660–2666.

[29] Agus, J., Kahar, P., Hyakutake, M, Tomizawa, S. et al., Unusual change in molecular weight of polyhydroxyalkanoate (PHA) during cultivation of PHA-accumulating *Escherichia coli*. Polym. Degrad. Stab. 2010, *95*, 2250–2254.

[30] Misra, S. K., Valappil, S. P., Roy, I., Boccaccini, A. R., Polyhydroxyalkanoate (PHA)/inorganic phase composites for tissue engineering applications. *Biomacromolecules* 2006, *7*, 2249–2258.

[31] Borschel, G. H., Kia, K. F., Kuzon, W. M. Jr., Dennis, R. G., Mechanical properties of acellular peripheral nerve. *J. Surg. Res.* 2003, *114*, 133–139.

[32] Kwan, M. K., Wall, E.J., Massie, J., Garfin, S. R., Strain, stress and stretch of peripheral nerve Rabbit experiments in vitro and in vivo. *Acta Orthop. Scand.* 1992, *63*, 267–272.

[33] Armstrong, S. J., Wiberg, M., Terenghi, G., Kingham, P. J., ECM molecules mediate both schwann cell proliferation and activation to enhance neurite outgrowth. *Tissue Eng.* 2007, *13*, 2863–2870.

[34] Binns, K. T., Taylor, P. P., Sicheri, F., Pawson, T. et al., Phosphorylation of tyrosine residues in the kinase domain and juxtamembrane region regulates the biological and catalytic activities of Eph receptors. *Mol. Cell. Biol.* 2000, *20*, 4791–4805.

[35] De Jaco, A., Comoletti, D., Kovarik, Z., Gaietta, G. et al., A Mutation linked with autism reveals a common mechanism of endoplasmic reticulum retention for the α,β-hydrolase fold protein family. *J. Biol. Chem.* 2006, *281*, 9667–9676.

[36] Tojima, T., Yamane, Y., Takahashi, M., Ito, E., Acquisition of neuronal proteins during differentiation of NG108-15 cells. *Neurosci. Res.* 2000, *37*, 153–161.

[37] Charness, M. E., Safran, R. M., Perides G., Ethanol inhibits neural cell-cell adhesion. *J. Biol. Chem.* 1994, *269*, 9304–9309.

[38] Hynes, R. O., Lander, A. D., Contact and adhesive specificities in the associations, migrations, and targeting of cells and axons. *Cell* 1992, *68*, 303–322.

[39] Hynes, R. O., Integrins: Bidirectional, allosteric signaling machines. *Cell* 2002, *110*, 673–687.

[40] Lee, J. W., Kim, Y. H., Park, K. D., Jee, K. S. et al., Importance of integrin β1-mediated cell adhesion on biodegradable polymers under serum depletion in mesenchymal stem cells and chondrocytes. *Biomaterials.* 2004, *25*, 1901–1909.

[41] Cargill, R. S. III, Dee, K. C., Malcolm, S., An assessment of the strength of NG108-15 cell adhesion to chemically modified surfaces. *Biomaterials* 1999, *20*, 2417–2425.